

# Nonconforming Maxwell Eigensolvers

Susanne C. Brenner\*    Fengyan Li<sup>†</sup>    Li-yeng Sung<sup>‡</sup>

May 23, 2008

## Abstract

Three Maxwell eigensolvers are discussed in this paper. Two of them use classical nonconforming finite element approximations, and the other is an interior penalty type discontinuous Galerkin method. A main feature of these solvers is that they are based on the formulation of the Maxwell eigenproblem on the space  $H_0(\text{curl}; \Omega) \cap H(\text{div}^0; \Omega)$ . These solvers are free of spurious eigenmodes and they do not require choosing penalty parameters. Furthermore, they satisfy optimal order error estimates on properly graded meshes, and their analysis is greatly simplified by the underlying compact embedding of  $H_0(\text{curl}; \Omega) \cap H(\text{div}^0; \Omega)$  in  $L_2(\Omega)$ . The performance and the relative merits of these eigensolvers are demonstrated through numerical experiments.

## Key Words

Maxwell eigenvalues, nonconforming finite element method, interior penalty method, spurious eigenvalues.

## 1 Introduction

The computation of Maxwell eigenvalues is of fundamental importance in computational electromagnetism. In this paper, we consider the following Maxwell eigenproblem with the perfectly conducting boundary condition:

---

\*Department of Mathematics and Center for Computation and Technology, Louisiana State University, Baton Rouge, LA 70803 (brenner@math.lsu.edu). The work of this author was supported in part by the National Science Foundation under Grant No. DMS-07-38028, and Grant No. DMS-07-13835.

<sup>†</sup>Department of Mathematical Sciences, Rensselaer Polytechnic Institute, Troy, NY, 12180 (lif@rpi.edu). The work of this author was supported in part by the National Science Foundation under Grant No. DMS-06-52481.

<sup>‡</sup>Department of Mathematics, Louisiana State University, Baton Rouge, LA 70803 (sung@math.lsu.edu). The work of this author was supported in part by the National Science Foundation under Grant No. DMS-07-13835.

Find  $(\hat{\mathbf{u}}, \lambda) \in H_0(\text{curl}; \Omega) \cap H(\text{div}^0; \Omega) \times \mathbb{R}$  such that  $\hat{\mathbf{u}} \neq \mathbf{0}$  and

$$(\nabla \times \hat{\mathbf{u}}, \nabla \times \mathbf{v}) = \lambda(\hat{\mathbf{u}}, \mathbf{v}) \quad \forall \mathbf{v} \in H_0(\text{curl}; \Omega) \cap H(\text{div}^0; \Omega). \quad (1.1)$$

Here  $\Omega \subset \mathbb{R}^2$  is a bounded polygonal domain,  $(\cdot, \cdot)$  denotes the  $L_2$  inner product, and

$$H(\text{curl}; \Omega) = \left\{ \mathbf{v} = \begin{bmatrix} v_1 \\ v_2 \end{bmatrix} \in [L_2(\Omega)]^2 : \nabla \times \mathbf{v} = \frac{\partial v_2}{\partial x_1} - \frac{\partial v_1}{\partial x_2} \in L_2(\Omega) \right\},$$

$$H(\text{div}; \Omega) = \left\{ \mathbf{v} = \begin{bmatrix} v_1 \\ v_2 \end{bmatrix} \in [L_2(\Omega)]^2 : \nabla \cdot \mathbf{v} = \frac{\partial v_1}{\partial x_1} + \frac{\partial v_2}{\partial x_2} \in L_2(\Omega) \right\},$$

$$H_0(\text{curl}; \Omega) = \{ \mathbf{v} \in H(\text{curl}; \Omega) : \mathbf{n} \times \mathbf{v} = 0 \text{ on } \partial\Omega \},$$

$$H(\text{div}^0; \Omega) = \{ \mathbf{v} \in H(\text{div}; \Omega) : \nabla \cdot \mathbf{v} = 0 \},$$

where  $\mathbf{n}$  is the unit outer normal on  $\partial\Omega$ .

Note that the eigenfunction  $\hat{\mathbf{u}}$  is subject to a divergence-free constraint, a property difficult to satisfy in numerical approximations. A common practice [6, 3, 13, 14, 24, 22, 25, 12, 7] in designing numerical schemes for (1.1) is to neglect the divergence-free condition and instead work with the following problem:

Find  $(\mathbf{u}, \lambda) \in H_0(\text{curl}; \Omega) \times \mathbb{R}$  such that  $\mathbf{u} \neq \mathbf{0}$  and

$$(\nabla \times \mathbf{u}, \nabla \times \mathbf{v}) = \lambda(\mathbf{u}, \mathbf{v}) \quad \forall \mathbf{v} \in H_0(\text{curl}; \Omega). \quad (1.2)$$

By doing so, a non-physical zero eigenvalue, whose eigenspace is of infinite dimension, is introduced into the spectrum. This in return requires that a successful numerical Maxwell eigensolver based on (1.2), in addition to being able to approximate the physical spectrum of (1.1), must also be able to separate the numerical approximations to the non-physical zero eigenvalue from those to the physical eigenvalues. Moreover, the non-compactness of the Maxwell operator based on (1.2) poses additional complexity in the analysis of the eigensolvers.

In this paper we work directly with (1.1). The eigensolvers we will present are closely related to the numerical schemes for the following curl-curl problem:

Given  $\mathbf{f} \in [L_2(\Omega)]^2$ , find  $\hat{\mathbf{u}} \in H_0(\text{curl}; \Omega) \cap H(\text{div}^0; \Omega)$  such that

$$(\nabla \times \hat{\mathbf{u}}, \nabla \times \mathbf{v}) + \alpha(\hat{\mathbf{u}}, \mathbf{v}) = (\mathbf{f}, \mathbf{v}) \quad \forall \mathbf{v} \in H_0(\text{curl}; \Omega) \cap H(\text{div}^0; \Omega), \quad (1.3)$$

where  $\alpha \in \mathbb{R}$ .

When  $\alpha = -\kappa^2$  with real wave number  $\kappa$ , the curl-curl problem (1.3) becomes the time-harmonic (frequency-domain) Maxwell equations formulated on  $H_0(\text{curl}; \Omega) \cap H(\text{div}^0; \Omega)$ , and it was solved in [9] by a locally

divergence-free nonconforming finite element method. The extension of the results in [9] to the case where  $\alpha > 0$  is straight-forward.

In [10, 11], two other schemes were proposed for solving the curl-curl problem (1.3). One is a locally divergence-free interior penalty method [10], and the other is a nonconforming finite element method that penalizes the divergence of the discrete solution [11]. Optimal order error estimates in both the  $L_2$  norm and the energy norm have been established for all three schemes in [9, 10, 11]. These schemes naturally define three numerical eigensolvers for (1.1), and the main goal of this paper is to study these eigensolvers analytically and numerically. A main feature of these solvers is that they are based on the formulation (1.1) instead of the formulation (1.2), and hence they are free of zero and nonzero spurious eigenmodes. The compactness of the underlying operator also greatly simplifies the analysis of these eigensolvers. Moreover these eigensolvers do not involve choosing any penalty parameters.

We have carried out numerical experiments that demonstrate the performance and the relative merits of these eigensolvers. Furthermore, we have conducted numerical tests to illustrate the roles played by various terms in the formulation of the solvers.

It turns out that some variants of the proposed eigensolvers generate spurious eigenmodes, and we have been able to detect them by certain numerical techniques. The related numerical tests, which may be of interest for other eigensolvers that generate spurious eigenmodes, are also reported.

The rest of the paper is organized as follows. The three eigensolvers are introduced in Section 2, and the optimal order convergence of these eigensolvers is established in Section 3. Results of a series of numerical experiments on the eigensolvers are reported in Section 4, and we discuss in Section 5 some numerical tests for the detection of spurious eigenmodes. We end with some concluding remarks in Section 6.

## 2 Numerical Schemes

We formulate three Maxwell eigensolvers for (1.1) in this section.

Let  $\mathcal{T}_h$  be a simplicial triangulation of  $\Omega$ . We denote a triangular element by  $T$ , the diameter of  $T$  by  $h_T$ , an edge by  $e$ , and the midpoint and length of  $e$  by  $m_e$  and  $|e|$ . The set of the edges of the triangles in  $\mathcal{T}_h$  is denoted by  $\mathcal{E}_h$ , and the set of the interior edges is denoted by  $\mathcal{E}_h^i$ . In order for the schemes to achieve optimal convergence for approximating the eigenvalues and eigenspaces, the triangulation  $\mathcal{T}_h$  must be properly graded around the corners of  $\Omega$ . We assume the following condition is satisfied by  $\mathcal{T}_h$ :

$$h_T \approx h\Phi_\mu(T) \quad \forall T \in \mathcal{T}_h. \quad (2.1)$$

Here  $h$  is the characteristic mesh size (for instance one can take  $h$  to be the largest diameter of  $T \in \mathcal{T}_h$ ) and the weight  $\Phi_\mu(T)$  is defined by

$$\Phi_\mu(T) = \prod_{l=1}^L |c_l - c_T|^{1-\mu_l}, \quad (2.2)$$

where  $c_T$  is the center of  $T$ , and  $\mu_l$  is the grading parameter chosen for each corner  $c_l$  of  $\Omega$  with interior angle  $\omega_l$  according to the following rules:

$$\mu_l = 1 \quad \text{if } \omega_l \leq \frac{\pi}{2}, \quad (2.3a)$$

$$\mu_l < \frac{\pi}{2\omega_l} \quad \text{if } \omega_l > \frac{\pi}{2}. \quad (2.3b)$$

For any  $e \subset \partial T$ , the following weight is equivalent to  $\Phi_\mu(T)$ :

$$\Phi_\mu(e) = \prod_{l=1}^L |c_l - m_e|^{1-\mu_l}.$$

**Remark 2.1.** The choices for the grading parameters are dictated by the singularities of the solution  $\hat{\mathbf{u}}$  of (1.1) and (1.3) around the corner  $c_l$  of  $\Omega$  [1, 18, 19]. According to (2.3) grading is needed at any corner  $c_l$  where the interior angle  $\omega_l$  is larger than  $\frac{\pi}{2}$ . This is different from problems involving the Laplace operator where grading is only needed at re-entrant corners, and it is due to the fact that the singularities of the curl-curl operator are one order worse than the singularities of the Laplace operator.

Since the jumps of vector fields across the edges of  $\mathcal{T}_h$  play an important role in the numerical schemes, we introduce the following notation: given a piecewise defined vector field  $\mathbf{v}$ , for any  $e \in \mathcal{E}_h^i$  shared by two triangles  $T_1$  and  $T_2$  with unit normals  $\mathbf{n}_1$  and  $\mathbf{n}_2$  of  $e$  pointing towards the outside of  $T_1$  and  $T_2$  respectively, we define

$$\begin{aligned} \llbracket \mathbf{v} \rrbracket_t &= \llbracket \mathbf{n} \times \mathbf{v} \rrbracket = (\mathbf{n}_1 \times \mathbf{v}_{T_1})|_e + (\mathbf{n}_2 \times \mathbf{v}_{T_2})|_e, \\ \llbracket \mathbf{v} \rrbracket_n &= \llbracket \mathbf{n} \cdot \mathbf{v} \rrbracket = (\mathbf{n}_1 \cdot \mathbf{v}_{T_1})|_e + (\mathbf{n}_2 \cdot \mathbf{v}_{T_2})|_e. \end{aligned}$$

Here  $\mathbf{v}_T = \mathbf{v}|_T$ , and we will refer to  $\llbracket \mathbf{v} \rrbracket_t$  and  $\llbracket \mathbf{v} \rrbracket_n$  as the tangential jump and the normal jump respectively.

For an edge  $e$  along  $\partial\Omega$ , we take  $\mathbf{n}_e$  to be the unit normal of  $e$  pointing towards the outside of  $\Omega$  and define

$$\llbracket \mathbf{v} \rrbracket_t = \llbracket \mathbf{n} \times \mathbf{v} \rrbracket = (\mathbf{n}_e \times \mathbf{v})|_e.$$

We also denote the piecewise defined curl operator and div operator by  $\nabla_h \times$  and  $\nabla_h \cdot$  respectively, i.e.,

$$(\nabla_h \times \mathbf{v})|_T = \nabla \times (\mathbf{v}|_T), \quad (\nabla_h \cdot \mathbf{v})|_T = \nabla \cdot (\mathbf{v}|_T).$$

We will use the following finite element spaces for the Maxwell eigensolvers. The first is the space  $W_h$  of Crouzeix-Raviart [20] non-conforming  $P_1$  vector fields:

$$W_h = \{\mathbf{v} \in [L_2(\Omega)]^2 : \mathbf{v}_T \in [P_1(T)]^2 \ \forall T \in \mathcal{T}_h, \mathbf{v} \text{ is continuous at the midpoints of the interior edges of } \mathcal{T}_h, \text{ and } \mathbf{n} \times \mathbf{v} = 0 \text{ at the midpoints of the edges of } \mathcal{T}_h \text{ along } \partial\Omega\}.$$

The second is the space  $V_h$  of locally divergence-free Crouzeix-Raviart non-conforming  $P_1$  vector fields:

$$V_h = \{\mathbf{v} \in W_h : \nabla \cdot \mathbf{v}_T = 0 \ \forall T \in \mathcal{T}_h\}.$$

The third is the space  $U_h$  of locally divergence-free piecewise (discontinuous)  $P_1$  vector fields:

$$U_h = \{\mathbf{v} \in [L_2(\Omega)]^2 : \mathbf{v}_T \in [P_1(T)]^2 \text{ and } \nabla \cdot \mathbf{v}_T = 0 \ \forall T \in \mathcal{T}_h\}.$$

We are now ready to define the three numerical eigensolvers for (1.1).

**Eigensolver 1:** Find  $(\hat{\mathbf{u}}_h, \lambda_h) \in V_h \times \mathbb{R}$  such that  $\hat{\mathbf{u}}_h \neq \mathbf{0}$  and

$$a_{h,0}(\hat{\mathbf{u}}_h, \mathbf{v}) = \lambda_h(\hat{\mathbf{u}}_h, \mathbf{v}), \quad \forall \mathbf{v} \in V_h, \quad (2.4)$$

where the bilinear form  $a_{h,0}(\mathbf{w}, \mathbf{v})$  is defined by

$$\begin{aligned} a_{h,0}(\mathbf{w}, \mathbf{v}) &= (\nabla_h \times \mathbf{w}, \nabla_h \times \mathbf{v}) + \sum_{e \in \mathcal{E}_h} \frac{[\Phi_\mu(e)]^2}{|e|} \int_e [[\mathbf{w}]]_t [[\mathbf{v}]]_t ds \\ &+ \sum_{e \in \mathcal{E}_h^i} \frac{[\Phi_\mu(e)]^2}{|e|} \int_e [[\mathbf{w}]]_n [[\mathbf{v}]]_n ds. \end{aligned} \quad (2.5)$$

**Eigensolver 2:** Find  $(\hat{\mathbf{u}}_h, \lambda_h) \in W_h \times \mathbb{R}$  such that  $\hat{\mathbf{u}}_h \neq \mathbf{0}$  and

$$b_{h,0}(\hat{\mathbf{u}}_h, \mathbf{v}) = \lambda_h(\hat{\mathbf{u}}_h, \mathbf{v}), \quad \forall \mathbf{v} \in W_h, \quad (2.6)$$

where the bilinear form  $b_{h,0}(\mathbf{w}, \mathbf{v})$  is defined by

$$\begin{aligned} b_{h,0}(\mathbf{w}, \mathbf{v}) &= (\nabla_h \times \mathbf{w}, \nabla_h \times \mathbf{v}) + \frac{1}{h^2} (\nabla_h \cdot \mathbf{w}, \nabla_h \cdot \mathbf{v}) \\ &+ \sum_{e \in \mathcal{E}_h} \frac{[\Phi_\mu(e)]^2}{|e|} \int_e [[\mathbf{w}]]_t [[\mathbf{v}]]_t ds \\ &+ \sum_{e \in \mathcal{E}_h^i} \frac{[\Phi_\mu(e)]^2}{|e|} \int_e [[\mathbf{w}]]_n [[\mathbf{v}]]_n ds. \end{aligned} \quad (2.7)$$

**Eigensolver 3:** Find  $(\hat{\mathbf{u}}_h, \lambda_h) \in U_h \times \mathbb{R}$  such that  $\hat{\mathbf{u}}_h \neq \mathbf{0}$  and

$$c_{h,0}(\hat{\mathbf{u}}_h, \mathbf{v}) = \lambda_h(\hat{\mathbf{u}}_h, \mathbf{v}), \quad \forall \mathbf{v} \in U_h, \quad (2.8)$$

where the bilinear form  $c_{h,0}(\mathbf{w}, \mathbf{v})$  is defined by

$$\begin{aligned} c_{h,0}(\mathbf{w}, \mathbf{v}) &= (\nabla_h \times \mathbf{w}, \nabla_h \times \mathbf{v}) + \sum_{e \in \mathcal{E}_h} \frac{[\Phi_\mu(e)]^2}{|e|} \int_e [[\mathbf{w}]]_t [[\mathbf{v}]]_t ds \\ &\quad + \sum_{e \in \mathcal{E}_h^i} \frac{[\Phi_\mu(e)]^2}{|e|} \int_e [[\mathbf{w}]]_n [[\mathbf{v}]]_n ds \\ &\quad + h^{-2} \sum_{e \in \mathcal{E}_h} \frac{1}{|e|} \int_e (\Pi_e^0 [[\mathbf{w}]]_t) (\Pi_e^0 [[\mathbf{v}]]_t) ds \\ &\quad + h^{-2} \sum_{e \in \mathcal{E}_h^i} \frac{1}{|e|} \int_e (\Pi_e^0 [[\mathbf{w}]]_n) (\Pi_e^0 [[\mathbf{v}]]_n) ds, \end{aligned} \quad (2.9)$$

and  $\Pi_e^0$  is the  $L_2$  orthogonal projection from  $L_2(e)$  onto the space  $P_0(e)$  of constant functions on  $e$ .

**Remark 2.2.** The following comments provide some intuitive motivations for the three Maxwell eigensolvers. More insights on various components of these schemes are provided by the numerical examples in Section 4.

1. Both Eigensolver 1 and Eigensolver 2 use classical nonconforming vector fields that have certain weak continuity. Eigensolver 3 is an interior penalty type discontinuous Galerkin method that uses completely discontinuous piecewise smooth vector fields. The last two terms in (2.9) compensate for the lack of any continuity in the discrete vector fields and they turn out to be necessary.
2. The divergence-free constraint in the eigenfunctions is imposed in Eigensolver 1 and Eigensolver 3 through the locally divergence-free condition in the definitions of  $V_h$  and  $U_h$ , and the same constraint is imposed in Eigensolver 2 through penalizing the divergence term in the bilinear form  $b_{h,0}$ . In all three solvers, certain consistency terms involving the jumps of both the normal and tangential components of the numerical solutions across element interfaces are also needed. These terms ensure that the inherent constraints for the space  $H_0(\text{curl}; \Omega) \cap H(\text{div}^0; \Omega)$  are satisfied by the discrete vector fields in a weak sense.
3. Each numerical eigensolver has its merits.

- In terms of the computational domain: the finite element space  $V_h$  for Eigensolver 1 does not have a completely local basis when the domain is multiply connected (right-hand side of Figure 4.3); but the finite element spaces  $W_h$  and  $U_h$  for Eigensolver 2 and Eigensolver 3 have completely local bases for general domains.
- In terms of the mesh: the weak continuity condition in the finite element spaces  $V_h$  and  $W_h$  for Eigensolver 1 and Eigensolver 2 require the meshes to be conforming; but the Eigensolver 3 can be applied to both conforming and nonconforming meshes (see Figure 4.1).
- In terms of the dimensions of the finite element spaces: the ratio of  $\dim V_h : \dim W_h : \dim U_h$  is approximately 2 : 3 : 5.

### 3 Error Analysis

In this section we give a unified error analysis for the three Maxwell eigensolvers. First we relate the Maxwell eigenproblem to the eigenproblem of a compact operator.

Given any  $\mathbf{f} \in [L_2(\Omega)]^2$ , we define  $T\mathbf{f} \in H_0(\text{curl}; \Omega) \cap H(\text{div}^0; \Omega)$  by the condition that

$$(\nabla \times (T\mathbf{f}), \nabla \times \mathbf{v}) + (T\mathbf{f}, \mathbf{v}) = (\mathbf{f}, \mathbf{v}) \quad (3.1)$$

for all  $\mathbf{v} \in H_0(\text{curl}; \Omega) \cap H(\text{div}^0; \Omega)$ , i.e.,  $T\mathbf{f}$  is the solution of (1.3) with  $\alpha = 1$ . Clearly  $T$  is a bounded linear operator from  $[L_2(\Omega)]^2$  into  $H_0(\text{curl}; \Omega) \cap H(\text{div}^0; \Omega)$ . Since  $H_0(\text{curl}; \Omega) \cap H(\text{div}^0; \Omega)$  is a compact subspace of  $[L_2(\Omega)]^2$  (cf. [16]), the operator  $T : [L_2(\Omega)]^2 \rightarrow [L_2(\Omega)]^2$  is symmetric, positive and compact. Moreover,  $(\hat{\mathbf{u}}, \lambda)$  satisfy (1.1) if and only if

$$T\hat{\mathbf{u}} = \frac{1}{1 + \lambda}\hat{\mathbf{u}}. \quad (3.2)$$

The eigenfunctions of  $T$  are precisely the Maxwell eigenfunctions.

Next we consider nonconforming approximations of  $T$  corresponding to the three schemes (2.4), (2.6) and (2.8).

Let  $Z_h$  be the finite element space  $V_h$ ,  $U_h$  or  $W_h$ , and  $\mathcal{N}_{h,0}(\cdot, \cdot)$  be the corresponding bilinear form  $a_{h,0}(\cdot, \cdot)$ ,  $b_{h,0}(\cdot, \cdot)$  or  $c_{h,0}(\cdot, \cdot)$ . The equations defining the three Maxwell eigensolvers can then be written as

$$\mathcal{N}_{h,0}(\hat{\mathbf{u}}_h, \mathbf{v}) = \lambda_h(\hat{\mathbf{u}}_h, \mathbf{v}) \quad \forall \mathbf{v} \in Z_h. \quad (3.3)$$

The discrete analog of  $T$  is the operator  $T_h : [L_2(\Omega)]^2 \rightarrow Z_h \subset [L_2(\Omega)]^2$  defined by

$$\mathcal{N}_{h,1}(T_h\mathbf{f}, \mathbf{v}) = (\mathbf{f}, \mathbf{v}) \quad \forall \mathbf{v} \in Z_h, \quad (3.4)$$

where

$$\mathcal{N}_{h,1}(\mathbf{w}, \mathbf{v}) = \mathcal{N}_{h,0}(\mathbf{w}, \mathbf{v}) + (\mathbf{w}, \mathbf{v}).$$

In other words  $T_h \mathbf{f} \in Z_h$  is the nonconforming finite element approximation of the solution  $T \mathbf{f}$  of the Maxwell source problem. Note that

$$T_h \hat{\mathbf{u}}_h = \frac{1}{1 + \lambda_h} \hat{\mathbf{u}}_h \quad (3.5)$$

is equivalent to (3.3). The eigenfunctions of  $T_h$  are precisely the discrete Maxwell eigenfunctions.

The following discretization error estimates for the Maxwell source problem have been derived in [9, 10, 11]:

$$\|(T - T_h) \mathbf{f}\|_{L_2(\Omega)} \leq C_\epsilon h^{2-\epsilon} \|\mathbf{f}\|_{L_2(\Omega)} \quad (3.6)$$

for all  $\mathbf{f} \in [L_2(\Omega)]^2$ , and

$$\|(T - T_h) \mathbf{f}\|_h \leq C_\epsilon h^{1-\epsilon} \|\mathbf{f}\|_{L_2(\Omega)} \leq C_\epsilon h^{1-\epsilon} \|\mathbf{f}\|_h \quad (3.7)$$

for all  $\mathbf{f} \in H_0(\text{curl}; \Omega) \cap H(\text{div}^0; \Omega) + Z_h$ , where  $\epsilon$  is an arbitrary positive constant and the mesh-dependent energy norm  $\|\cdot\|_h$  is defined by

$$\|\mathbf{v}\|_h^2 = \mathcal{N}_{h,1}(\mathbf{v}, \mathbf{v}).$$

The uniform estimates (3.6) and (3.7) imply that the classical theory of spectral approximation [23, 15, 2] can be applied to the nonconforming Maxwell eigensolvers.

**Theorem 3.1.** Let  $0 \leq \lambda_1 \leq \lambda_2 \leq \dots$  be the eigenvalues of (1.1),  $\lambda = \lambda_j = \lambda_{j+1} = \dots = \lambda_{j+m-1}$  be an eigenvalue with multiplicity  $m$ , and  $Z_\lambda \subset H_0(\text{curl}; \Omega) \cap H(\text{div}^0; \Omega)$  be the corresponding  $m$  dimensional eigenspace. Let  $0 \leq \lambda_{h,1} \leq \lambda_{h,2} \leq \dots$  be the eigenvalues obtained by one of the three eigensolvers. Then as  $h \downarrow 0$ , we have

$$|\lambda_{h,l} - \lambda| \leq C_{\lambda, d_\lambda, \epsilon} h^{2-\epsilon} \quad l = j, j+1, \dots, j+m-1, \quad (3.8)$$

where  $d_\lambda$  is the distance from  $\lambda$  to the other Maxwell eigenvalues and  $\epsilon$  is an arbitrary positive number.

Furthermore, if  $Z_{h,\lambda}$  is the space spanned by the discrete Maxwell eigenfunctions corresponding to  $\lambda_{h,j}, \dots, \lambda_{h,j+m-1}$ , then the gap between  $Z_\lambda$  and  $Z_{h,\lambda}$  goes to zero at the rate of  $C_{\lambda, d_\lambda, \epsilon} h^{2-\epsilon}$  in the  $L_2$  norm and at the rate of  $C_{\lambda, d_\lambda, \epsilon} h^{1-\epsilon}$  in the energy norm  $\|\cdot\|_h$ .

*Proof.* Let  $1 \geq \mu_1 \geq \mu_2 \geq \dots$  be the eigenvalues of  $T$  and  $1 \geq \mu_{h,1} \geq \mu_{h,2} \geq \dots$  be the eigenvalues of  $T_h$ . In view of the relations (3.2) and (3.5), it is equivalent to establish the convergence of  $\mu_{h,j}$  to  $\mu_j$ .

Let  $\mu$  be an eigenvalue of  $T$  of multiplicity  $m$  corresponding to the Maxwell eigenvalue  $\lambda$ . The  $L_2$  orthogonal projection  $E_\mu$  onto the eigenspace  $Z_\mu = Z_\lambda$  is given by the contour integral [21]

$$E_\mu = \frac{1}{2\pi i} \int_{C_{\mu, \delta_\mu}} (\mu I - T)^{-1} d\mu, \quad (3.9)$$

where  $I$  is the identity operator on  $[L_2(\Omega)]^2$ ,  $C_{\mu, \delta_\mu}$  is the counterclockwise oriented circle centered at  $\mu$  with radius  $\delta_\mu$ , and  $\delta_\mu$  is small enough so that  $\mu$  is the only eigenvalue of  $T$  inside and on  $C_{\mu, \delta_\mu}$ .

For  $h$  sufficiently small, the operator  $\mu I - T_h$  is invertible on  $C_{\mu, \delta_\mu}$  and we can define the  $L_2$  orthogonal projection  $E_{h, \mu}$  by

$$E_{h, \mu} = \frac{1}{2\pi i} \int_{C_{\mu, \delta_\mu}} (\mu I - T_h)^{-1} d\mu. \quad (3.10)$$

The space  $Z_{h, \mu} = Z_{h, \lambda} = E_{h, \mu}[L_2(\Omega)]^2$  is spanned by the eigenfunctions of  $T_h$  corresponding to eigenvalues of  $T_h$  inside  $C_{\mu, \delta_\mu}$ .

It follows from (3.6), (3.9) and (3.10) that

$$\|(E_\lambda - E_{h, \lambda})\mathbf{w}\|_{L_2(\Omega)} \leq C_{\delta_\mu, \epsilon} h^{2-\epsilon} \|\mathbf{w}\|_{L_2(\Omega)} \quad (3.11)$$

for all  $\mathbf{w} \in [L_2(\Omega)]^2$  and

$$\|(E_\lambda - E_{h, \lambda})\mathbf{w}\|_h \leq C_{\delta_\mu, \epsilon} h^{1-\epsilon} \|\mathbf{w}\|_h \quad (3.12)$$

for all  $\mathbf{w} \in H_0(\text{curl}; \Omega) \cap H(\text{div}^0; \Omega) + Z_h$ .

Hence, for  $h$  sufficiently small, the rank of  $E_{h, \mu}$  is  $m$  and there are exactly  $m$  eigenvalues (counting multiplicity) of  $T_h$  inside the circle  $C_{\mu, \delta_\mu}$ . To complete the proof of the first part of the theorem, it only remains to estimate  $|\mu - \mu_h|$ , where  $\mu_h$  is any one of the eigenvalues of  $T_h$  inside  $C_{\mu, \delta_\mu}$ .

Let  $\mathbf{x} \in Z_{h, \lambda}$  be a unit eigenfunction of  $\mu_h$ . Then we have

$$(T_h \mathbf{x}, \mathbf{x}) = \mu_h \quad \text{and} \quad \|\mathbf{x}\|_{L_2(\Omega)} = 1. \quad (3.13)$$

Let  $\hat{\mathbf{x}} = E_\lambda \mathbf{x}$  and  $\hat{\mathbf{y}} = \mathbf{x} - \hat{\mathbf{x}}$ . Then  $\hat{\mathbf{x}}$  and  $\hat{\mathbf{y}}$  are orthogonal with respect to both the  $L_2$  inner product and the inner product  $(T \cdot, \cdot)$ , and the estimate (3.11) implies that

$$\|\hat{\mathbf{y}}\|_{L_2(\Omega)} = \|(E_\lambda - E_{h, \lambda})\mathbf{x}\|_{L_2(\Omega)} \leq C_{\delta_\mu, \epsilon} h^{2-\epsilon}. \quad (3.14)$$

Hence it follows from Pythagoras' theorem with respect to the  $L_2$  inner product that

$$1 - \|\hat{\mathbf{x}}\|_{L_2(\Omega)}^2 = \|\mathbf{x}\|_{L_2(\Omega)}^2 - \|\hat{\mathbf{x}}\|_{L_2(\Omega)}^2 = \|\hat{\mathbf{y}}\|_{L_2(\Omega)}^2 \leq C_{\delta_\mu, \epsilon} h^{4-\epsilon}. \quad (3.15)$$

In particular we have  $\hat{\mathbf{x}} \neq \mathbf{0}$  for  $h$  sufficiently small.

Let  $\hat{e} = \hat{\boldsymbol{x}}/\|\hat{\boldsymbol{x}}\|_{L_2(\Omega)}$ . Then  $\hat{e}$  is a unit eigenfunction of  $T$  for the eigenvalue  $\mu$ , and we have, by (3.13),

$$\begin{aligned} |\mu - \mu_h| &= |(T\hat{e}, \hat{e}) - (T_h\boldsymbol{x}, \boldsymbol{x})| \\ &\leq |((T - T_h)\boldsymbol{x}, \boldsymbol{x})| + |(T\hat{e}, \hat{e}) - (T\boldsymbol{x}, \boldsymbol{x})|. \end{aligned} \quad (3.16)$$

From (3.6) we have

$$|((T - T_h)\boldsymbol{x}, \boldsymbol{x})| \leq C_\epsilon h^{2-\epsilon}, \quad (3.17)$$

and it follows from Pythagoras' theorem with respect to the inner product  $(T\cdot, \cdot)$  that

$$\begin{aligned} |(T\hat{e}, \hat{e}) - (T\boldsymbol{x}, \boldsymbol{x})| &= |(T\hat{e}, \hat{e}) - (T\hat{\boldsymbol{x}}, \hat{\boldsymbol{x}}) - (T\hat{\boldsymbol{y}}, \hat{\boldsymbol{y}})| \\ &\leq (1 - \|\hat{\boldsymbol{x}}\|_{L_2(\Omega)}^2)(T\hat{e}, \hat{e}) + (T\hat{\boldsymbol{y}}, \hat{\boldsymbol{y}}). \end{aligned} \quad (3.18)$$

Combining (3.14), (3.15) and (3.18), we find

$$|(T\hat{e}, \hat{e}) - (T\boldsymbol{x}, \boldsymbol{x})| \leq C_{\delta_\mu, \epsilon} h^{4-\epsilon},$$

which together with (3.16) and (3.17) implies

$$|\mu - \mu_h| \leq C_{\delta_\mu, \epsilon} h^{2-\epsilon}. \quad (3.19)$$

The estimate (3.8) follows from (3.19) and the relations

$$\mu_j = 1/(1 + \lambda_j) \quad \text{and} \quad \mu_{h,j} = 1/(1 + \lambda_{h,j}).$$

Finally, we recall that the gap  $\hat{\delta}(M, N)$  between two subspaces  $M$  and  $N$  of a normed linear space  $(X, \|\cdot\|_X)$  is defined by (cf. [23])

$$\hat{\delta}(M, N) = \max(\delta(M, N), \delta(N, M)),$$

where

$$\delta(M, N) = \sup_{\substack{x \in M \\ \|x\|_X = 1}} \inf_{y \in N} \|x - y\|_X.$$

Therefore the statements about the gap between  $Z_\lambda = Z_\mu$  and  $Z_{h,\lambda} = Z_{h,\mu}$  follow immediately from (3.11) and (3.12).  $\square$

**Remark 3.2.** Because of the graded mesh, the error estimates in Theorem 3.1 are optimal even when the Maxwell eigenfunctions do not have full regularity, which may happen when one of the interior angles of the computational domain is larger than  $\frac{\pi}{2}$ .

**Remark 3.3.** The compactness of the solution operator  $T$  and the existence of the uniform estimates (3.6) and (3.7) greatly simplify the analysis of the three nonconforming Maxwell eigensolvers. In comparison the analysis of Maxwell eigensolvers [5, 6, 3, 13, 14, 4, 12, 7] based on (1.2) is much more involved.

## 4 Numerical Results

In this section we report the results of a series of numerical experiments on the three nonconforming Maxwell eigensolvers. They confirm the theoretical results, demonstrate the relative merits of each eigensolver, and illustrate the roles played by various terms in the formulations of the eigensolvers. In all the plots, the symbol “o” denotes the exact eigenvalue, and “(2)” indicates that the multiplicity of the eigenvalue is 2.

The following examples are considered throughout this section:

**Example 1.** We take the computational domain to be the square

$$\Omega = (0, \pi)^2.$$

The exact Maxwell eigenvalues on this domain are given by  $r^2 + s^2$ , where  $r, s = 0, 1, 2, 3, 4, \dots$  and  $r^2 + s^2 > 0$ . For instance, the first 10 eigenvalues are 1, 1, 2, 4, 4, 5, 5, 8, 9, 9. The eigenfunctions are  $H^2$  functions.

**Example 2.** We take the computational domain to be the L-shaped domain (Figure 4.3, left)

$$\Omega = (-0.5, 0.5)^2 \setminus [0, 0.5]^2.$$

Based on Dauge’s benchmark examples for the Maxwell eigenproblem (<http://perso.univ-rennes1.fr/monique.dauge/core/index.html>), the values of the first 5 eigenvalues are 5.90248729632, 14.13612546712, 39.47841760436, 39.47841760436 and 45.5579175916. It is also known from the same source that the 1<sup>st</sup> and 5<sup>th</sup> Maxwell eigenfunctions have a strong unbounded singularity, the 2<sup>nd</sup> one belongs to  $H^1(\Omega)$ , and the 3<sup>rd</sup> and the 4<sup>th</sup> ones are analytic.

**Example 3.** We take the computational domain to be the doubly connected domain (Figure 4.3, right)

$$\Omega = (0, 4)^2 \setminus [1, 3]^2.$$

The smallest Maxwell eigenvalue on this domain is 0 with multiplicity 1. The corresponding eigenfunction is defined by  $\hat{\mathbf{u}} = \nabla\phi$ , where  $\phi \in H^1(\Omega)$  satisfies

$$\begin{aligned} -\Delta\phi &= 0 \quad \text{in } \Omega, \\ \phi|_{\Gamma_{int}} &= 0, \quad \phi|_{\Gamma_{ext}} = 1, \end{aligned}$$

and  $\Gamma_{int}$  (resp.  $\Gamma_{ext}$ ) is the boundary of  $[1, 3]^2$  (resp.  $[0, 4]^2$ ).

The characteristic mesh size  $h$  for the numerical experiments is chosen as follows. For Example 1, we take  $h = \pi/n$ , where  $n$  is the number of the subintervals along  $[0, \pi] \times \{y = 0\}$ , for the conforming and nonconforming meshes in Figure 4.1. For Example 2, we take  $h = 1/(2n)$ , where  $n$  is the number of the subintervals along  $[-0.5, 0] \times \{y = 0.5\}$ , for the mesh in Figure 4.3 (left). For Example 3, we take  $h = 4/n$ , where  $n$  is the number of the subintervals along  $[0, 4] \times \{y = 0\}$ , for the mesh in Figure 4.3 (right).

## 4.1 Numerical results for Eigensolver 1

In this subsection we present numerical results on the accuracy of the Eigensolver 1 and on the roles played by the consistency terms.

### 4.1.1 Accuracy of the scheme

In the first experiment we compute the Maxwell eigenvalues on the square  $(0, \pi)^2$  using the uniform meshes depicted in Figure 4.1 (left).

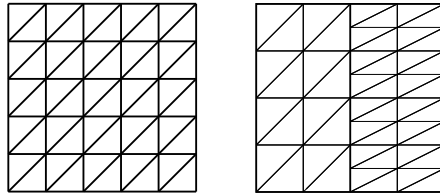


Figure 4.1: Conforming uniform mesh (left) and nonconforming mesh (right) on the square domain  $(0, \pi)^2$

We plot the first 20 numerical eigenvalues versus the parameter  $n = \pi/h$  in Figure 4.2, from which one can see that the eigenvalues are well resolved

even when the meshes are still coarse and there is no spurious eigenmode. The numerical approximations converge with second order accuracy which confirms the error estimate (3.8). To save space, only the first 5 numerical eigenvalues and their convergence rates are included in Table 4.1.

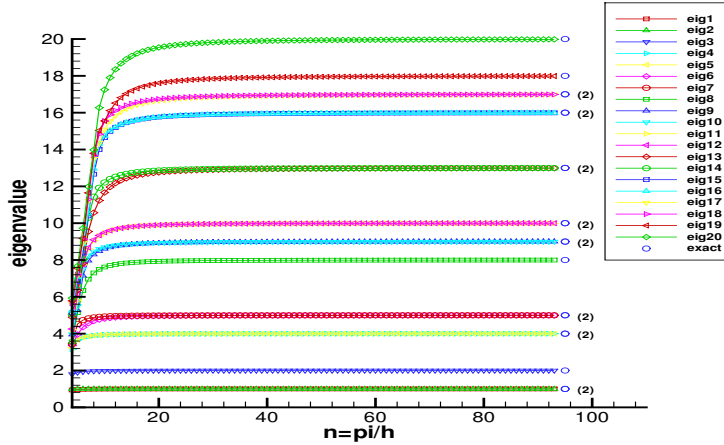


Figure 4.2: First 20 numerical Maxwell eigenvalues computed by Eigensolver 1 on  $(0, \pi)^2$  with conforming uniform meshes

Table 4.1: First 5 numerical Maxwell eigenvalues computed by Eigensolver 1 on  $(0, \pi)^2$  with conforming uniform meshes.

$n = \frac{\pi}{h}$	the 1 <sup>st</sup>	order	the 2 <sup>nd</sup>	order	the 3 <sup>rd</sup>	order	the 4 <sup>th</sup>	order	the 5 <sup>th</sup>	order
4	0.943	-	1.000	-	1.800	-	3.154	-	3.238	-
8	0.988	2.19	1.000	-0.67	1.967	2.60	3.895	3.01	3.896	2.87
16	0.997	2.07	1.000	1.26	1.993	2.26	3.977	2.21	3.977	2.20
32	0.999	2.03	1.000	1.72	1.998	2.11	3.995	2.08	3.995	2.08
64	1.000	2.01	1.000	1.87	2.000	2.05	3.999	2.03	3.999	2.03
128	1.000	2.01	1.000	1.94	2.000	2.03	4.000	2.01	4.000	2.01
Exact	1		1		2		4		4	

In the second experiment we compute the Maxwell eigenvalues for the  $L$ -shaped domain  $(-0.5, 0.5)^2 \setminus [0, 0.5]^2$  using the graded meshes depicted in Figure 4.3 (left), where the grading parameter at the re-entrant corner is chosen to be  $\frac{1}{3}$ .

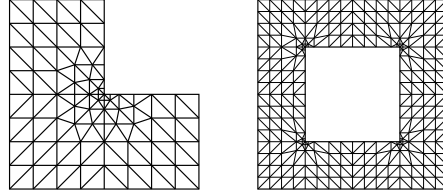


Figure 4.3: Graded meshes on the L-shaped domain  $(-0.5, 0.5)^2 \setminus [0, 0.5]^2$  (left) and on the doubly connected domain  $(0, 4)^2 \setminus [1, 3]^2$  (right)

Table 4.2 contains the numerical results for the first 5 Maxwell eigenvalues. One can see that our method has second order accuracy, on relatively coarse meshes and for eigenfunctions with very different regularity. In Figure 4.4 we plot the first 10 numerical eigenvalues versus  $n = 1/(2h)$ , which clearly demonstrates the absence of any spurious eigenmodes.

Table 4.2: First 5 numerical Maxwell eigenvalues computed by Eigensolver 1 on the L-shaped domain using graded meshes

$n = \frac{1}{2h}$	the 1 <sup>st</sup>	order	the 2 <sup>nd</sup>	order	the 3 <sup>rd</sup>	order	the 4 <sup>th</sup>	order	the 5 <sup>th</sup>	order
4	5.319	-	10.727	-	11.276	-	11.441	-	12.350	-
8	5.756	1.99	13.532	2.50	31.448	1.81	37.652	3.94	39.529	2.46
16	5.867	2.05	13.992	2.07	37.307	1.89	39.100	2.27	44.429	2.42
32	5.894	2.08	14.101	2.03	38.929	1.98	39.390	2.10	45.291	2.08
64	5.901	2.09	14.127	2.01	39.341	2.00	39.457	2.05	45.493	2.03
Exact	5.902		14.136		39.478		39.478		45.558	

#### 4.1.2 The role of the consistency terms

In order for a numerical scheme to be successful for either the Maxwell source problem or the Maxwell eigenproblem, the correct amount of continuity for the tangential and/or the normal component of the discrete vector fields must be imposed across element interfaces. If the continuity is over-imposed, the scheme may generate a sequence of approximations that converge to a wrong solution [6, 24]. On the other hand, if the continuity is under-imposed, the scheme may not converge [9]. In this subsection we will demonstrate numerically that the correct amount of continuity is imposed by Eigensolver 1.

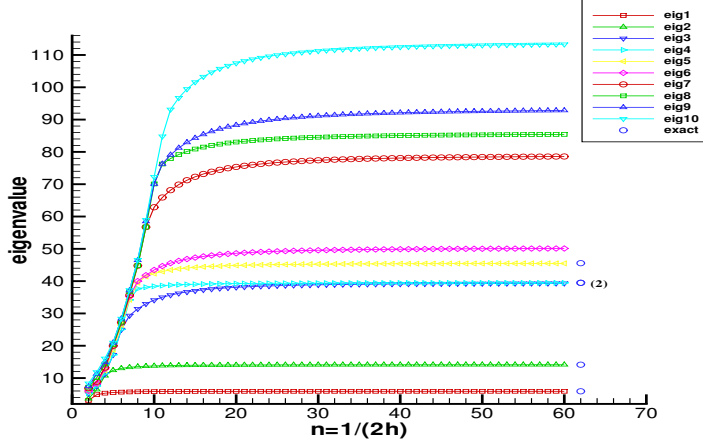


Figure 4.4: First 10 Maxwell eigenvalues computed by Eigensolver 1 on the L-shaped domain using graded meshes

For this purpose we rewrite the bilinear form  $a_{h,0}(\mathbf{w}, \mathbf{v})$  as

$$\begin{aligned}
 a_{h,0}(\mathbf{w}, \mathbf{v}) &= (\nabla_h \times \mathbf{w}, \nabla_h \times \mathbf{v}) + C_{p,t} \sum_{e \in \mathcal{E}_h} \frac{[\Phi_\mu(e)]^2}{|e|} \int_e [[\mathbf{w}]]_t [[\mathbf{v}]]_t ds \\
 &\quad + C_{p,n} \sum_{e \in \mathcal{E}_h^i} \frac{[\Phi_\mu(e)]^2}{|e|} \int_e [[\mathbf{w}]]_n [[\mathbf{v}]]_n ds, \tag{4.1}
 \end{aligned}$$

where we take  $C_{p,n} = C_{p,t} = 1$  in (2.5). Here  $\sum_{e \in \mathcal{E}_h} \frac{[\Phi_\mu(e)]^2}{|e|} \int_e [[\mathbf{w}]]_t [[\mathbf{v}]]_t ds$  is a consistency term involving the *tangential* jumps of the discrete vector fields across element interfaces, and  $\sum_{e \in \mathcal{E}_h^i} \frac{[\Phi_\mu(e)]^2}{|e|} \int_e [[\mathbf{w}]]_n [[\mathbf{v}]]_n ds$  is a consistency term involving the *normal* jumps.

From Figure 4.5 we see that if we simply remove either the tangential consistency term or the normal one from our solver, i.e., if we take  $C_{p,n} = 0, C_{p,t} = 1$  (T-type variant) or  $C_{p,n} = 1, C_{p,t} = 0$  (N-type variant) in (4.1), then spurious eigenmodes will appear. In particular, zero spurious eigenmodes are generated by the N-type variant. Similar results are also observed on the L-shaped domain.

We have also tested the effects of different choices of the penalty parameters  $C_{p,n}$  and  $C_{p,t}$  on the performance of the eigensolver on the square  $(0, \pi)^2$ . From the plots in Figure 4.6 we can see that the performance of the eigensolver containing both consistency terms (TN-type variant) is not

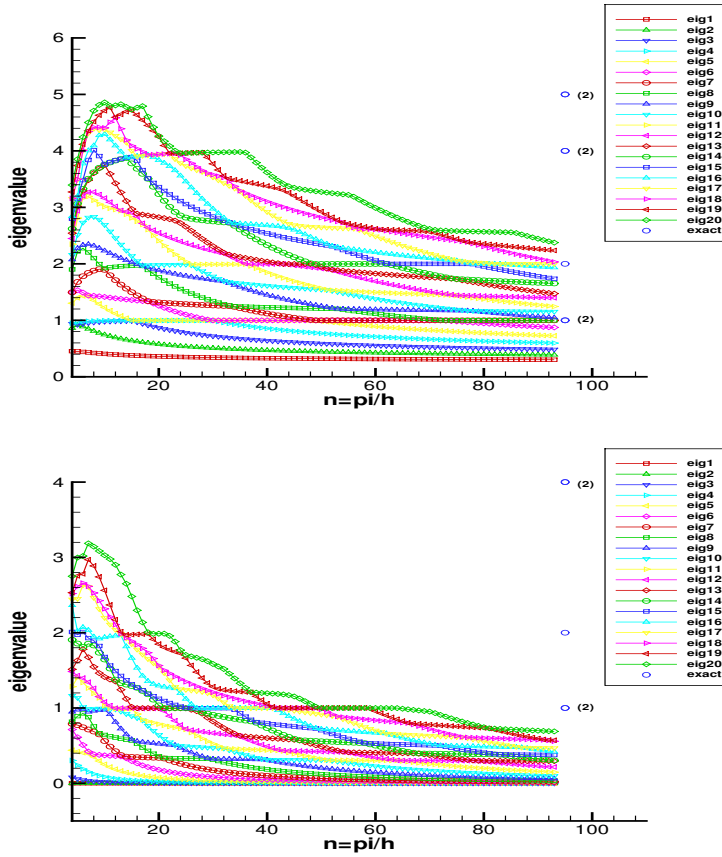


Figure 4.5: Maxwell eigenvalues on the square  $(0, \pi)^2$  computed by the *T-type* variant (top,  $C_{p,n} = 0, C_{p,t} = 1$ ) and the *N-type* variant (bottom,  $C_{p,n} = 1, C_{p,t} = 0$ ) of Eigensolver 1 using conforming uniform meshes

sensitive to the values of  $C_{p,n}$  and  $C_{p,t}$ . On the other hand the performance of the T-type variant improves dramatically with a large  $C_{p,t}$ . The lower range of the spectrum is well-captured (indeed with second order accuracy). However, some nonzero spurious eigenvalues still exist for a fixed  $C_{p,t}$ . The performance of the N-type variant also improves with a larger  $C_{p,n}$ . But many spurious eigenmodes still persist.

We have carried out similar experiments for the L-shaped domain using

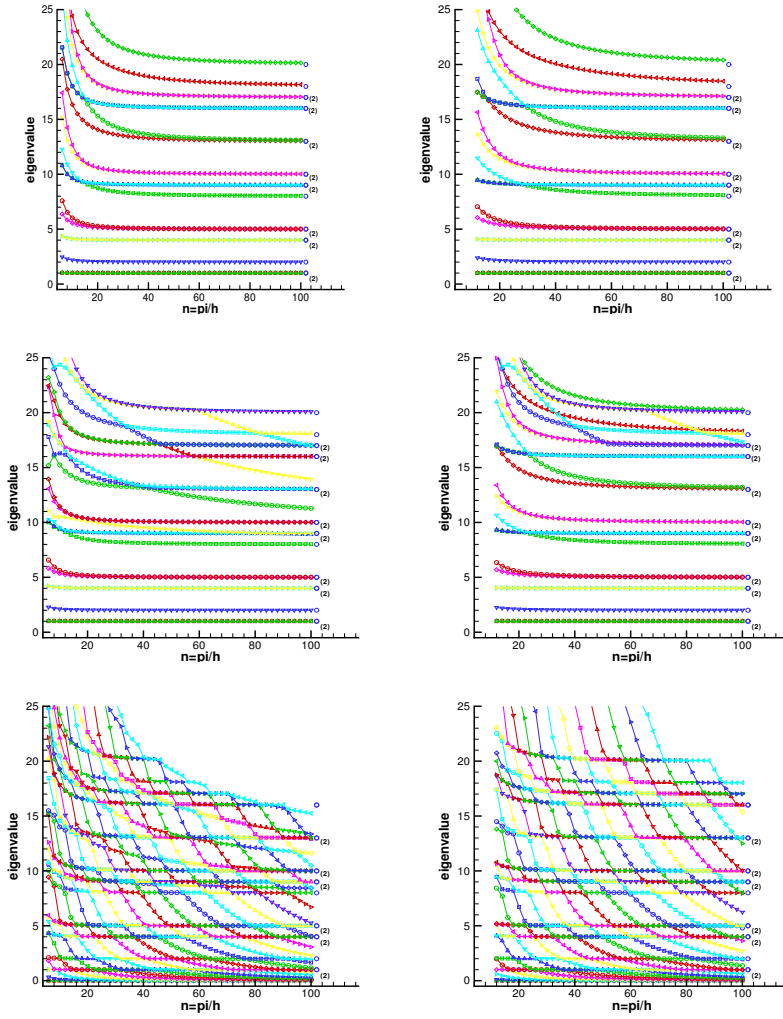


Figure 4.6: Maxwell eigenvalues (from top to bottom) for the square  $(0, \pi)^2$  computed by TN-type ( $C_{p,n} = C_{p,t} = C_p$ ), T-type ( $C_{p,n} = 0, C_{p,t} = C_p$ ) and N-type ( $C_{p,n} = C_p, C_{p,t} = 0$ ) variants of Eigensolver 1 using conforming uniform meshes, where  $C_p = 30$  on the left and  $C_p = 100$  on the right

graded meshes. From the plots in Figure 4.7 we see that both the T-type

and the N-type variants perform well for relatively large penalty parameters, though the N-type variant still produces 3 spurious zero eigenvalues.

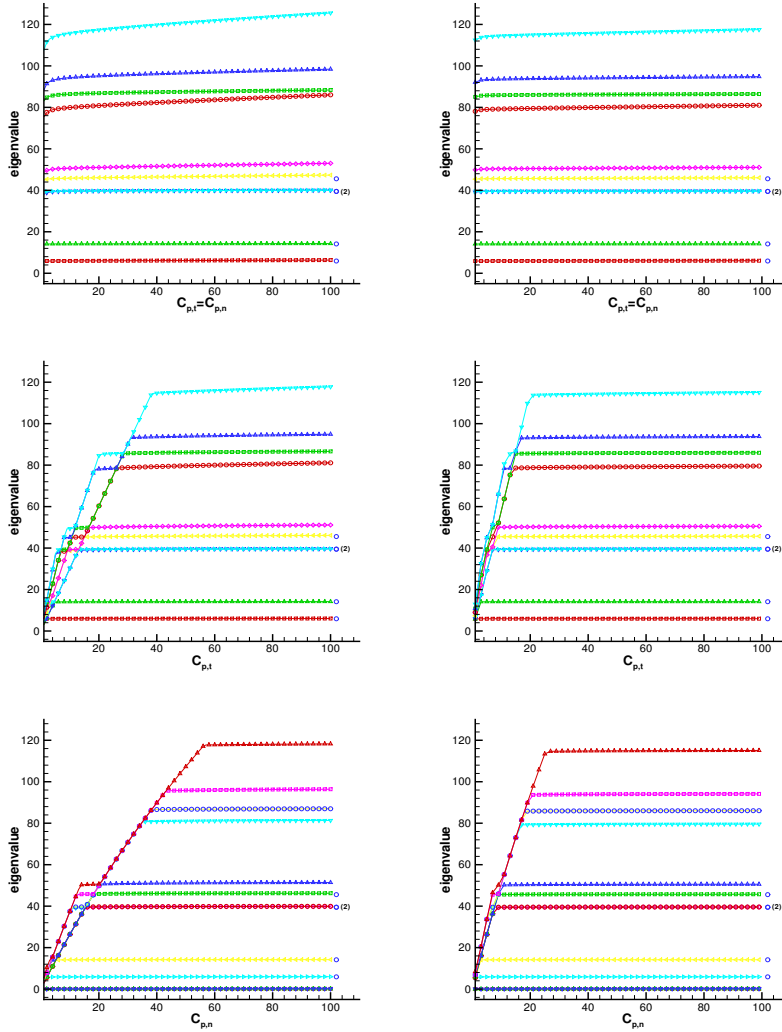


Figure 4.7: Maxwell eigenvalues (from top to bottom) for the L-shaped domain computed by TN-type ( $C_{p,n} = C_{p,t} = C_p$ ), T-type ( $C_{p,n} = 0, C_{p,t} = C_p$ ) and N-type ( $C_{p,n} = C_p, C_{p,t} = 0$ ) variants of Eigensolver 1 using graded meshes, where  $C_p = 25$  on the left and  $C_p = 50$  on the right

From the numerical study we can conclude that (i) Eigensolver 1 imposes the correct amount of continuity through the two consistency terms and it is optimal without having to choose any penalty parameters; (ii) the tangential consistency term is necessary for removing the zero spurious eigenmodes; (iii) a large  $C_{p,t}$  (resp.  $C_{p,n}$ ) can improve the performance of the T-type (resp. N-type) variant.

In Section 5 we will present some numerical techniques that can detect the spurious eigenmodes generated by the T-type and N-type variants.

## 4.2 Numerical results for Eigensolver 2

In this subsection we present numerical results for Eigensolver 2. We will focus on the accuracy of the scheme, the role of the weight for the divergence term in  $b_{h,0}(\cdot, \cdot)$ , and the performance of the scheme for the doubly connected domain. Results similar to those reported in Section 4.1.2 for Eigensolver 1 also holds for Eigensolver 2 and will not be repeated here.

### 4.2.1 Accuracy of the scheme

In the first experiment we compute the Maxwell eigenvalues for the square  $(0, \pi)^2$  using uniform meshes. In the top of Figure 4.9, we plot the numerical results of the first 20 eigenvalues versus the parameter  $n = \pi/h$ , from which one can see that the eigenvalues are well resolved even for very coarse meshes and there is no spurious eigenmode. The numerical approximations converge with second order accuracy, which confirms the error estimate (3.8). To save space, only the first 5 numerical eigenvalues and their convergence rates are reported in Table 4.3.

Table 4.3: First 5 Maxwell eigenvalues on  $(0, \pi)^2$  computed by Eigensolver 2 using conforming uniform meshes

$n = \frac{\pi}{h}$	the 1 <sup>st</sup>	order	the 2 <sup>nd</sup>	order	the 3 <sup>rd</sup>	order	the 4 <sup>th</sup>	order	the 5 <sup>th</sup>	order
4	0.943	-	1.000	-	1.798	-	2.647	-	3.145	-
8	0.988	2.19	1.000	-0.40	1.967	2.60	3.895	3.69	3.896	3.04
16	0.997	2.07	1.000	1.26	1.993	2.27	3.977	2.21	3.977	2.20
32	0.999	2.03	1.000	1.72	1.998	2.12	3.995	2.08	3.995	2.08
64	1.000	2.01	1.000	1.87	2.000	2.05	3.999	2.03	3.999	2.03
128	1.000	2.01	1.000	1.94	2.000	2.03	4.000	2.01	4.000	2.01
Exact	1		1		2		4		4	

In the second experiment, we compute the Maxwell eigenvalues for the  $L$ -shaped domain, where the meshes are graded around the re-entrant corner with grading parameter  $\frac{1}{3}$ . Table 4.4 contains the first 5 numerical

eigenvalues, from which one can see that the scheme has second order accuracy on relatively coarse meshes. In Figure 4.8 we plot the first 10 numerical eigenvalues versus  $n = 1/(2h)$ , which shows the absence of spurious eigenmodes.

Note that Table 4.1 and Table 4.3 give almost identical results, and so do Table 4.2 and Table 4.4.

Table 4.4: First 5 Maxwell eigenvalues for the L-shaped domain computed by Eigensolver 2 using graded meshes

$n = \frac{1}{2h}$	the 1 <sup>st</sup>	order	the 2 <sup>nd</sup>	order	the 3 <sup>rd</sup>	order	the 4 <sup>th</sup>	order	the 5 <sup>th</sup>	order
4	5.319	-	10.726	-	11.275	-	11.440	-	12.349	-
8	5.756	1.99	13.532	2.50	31.448	1.81	37.651	3.94	39.529	2.46
16	5.867	2.05	13.992	2.07	37.307	1.89	39.100	2.27	44.429	2.42
32	5.894	2.08	14.101	2.03	38.929	1.98	39.390	2.10	45.291	2.08
64	5.901	2.08	14.127	2.01	39.341	2.00	39.457	2.05	45.493	2.03
Exact	5.902		14.136		39.478		39.478		45.558	

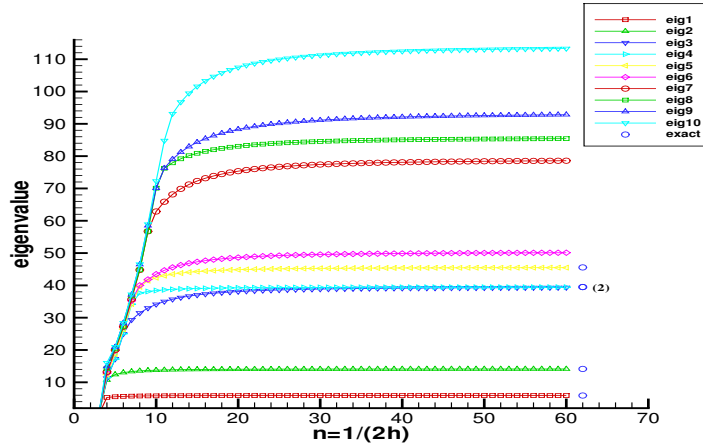


Figure 4.8: First 10 Maxwell eigenvalues for the L-shaped domain computed by Eigensolver 2 using graded meshes

#### 4.2.2 The weight for the divergence term in (2.7)

The divergence-free constraint is imposed on Eigensolver 2 through the weight  $h^{-2}$  for the divergence term in (2.7). Here we explore the variant

where the weight is  $h^{-1}$  by comparing in Figure 4.9 the first 20 Maxwell eigenvalues for the square  $(0, \pi)^2$  computed by the two schemes using conforming uniform meshes.

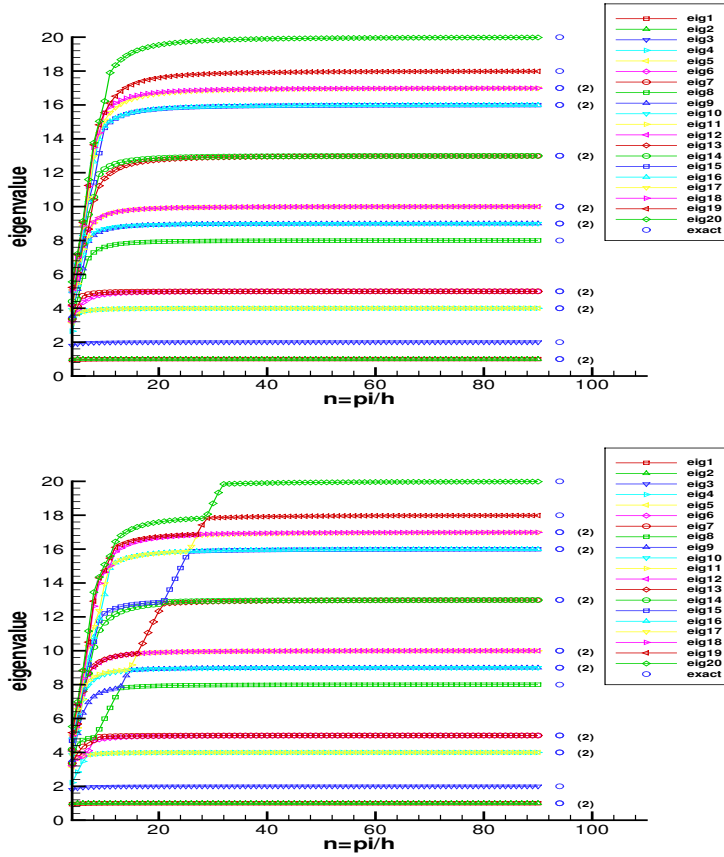


Figure 4.9: First 20 Maxwell eigenvalues for the square computed by Eigensolver 2 (top) and the variant where the weight for the divergence term is  $h^{-1}$  (bottom), using conforming uniform meshes

Based on these plots, the following comments can be made.

1. The lower ranges of the numerical spectra computed by Eigensolver 2 and the variant are almost identical.
2. Eigensolver 2 can resolve the eigenvalues of different magnitudes very well even on relatively coarse meshes. For a large eigenvalue the

same level of resolution can only be achieved by the variant on finer meshes. This is confirmed further by the numerical results for the next 20 Maxwell eigenvalues (which are not reported).

We can understand these observations by considering the following eigenproblem: Find  $(\mathbf{u}, \lambda) \in H_0(\text{curl}; \Omega) \cap H(\text{div}^0; \Omega)$  such that

$$(\nabla \times \mathbf{u}, \nabla \times \mathbf{v}) + \gamma(\nabla \cdot \mathbf{u}, \nabla \cdot \mathbf{v}) = \lambda(\mathbf{u}, \mathbf{v}), \quad (4.2)$$

for all  $H_0(\text{curl}; \Omega) \cap H(\text{div}^0; \Omega)$ . It follows from the results in [8] that this eigenproblem can be solved with second order accuracy using the finite element space  $W_h$  by replacing the weight  $h^{-2}$  in  $b_{h,0}(\cdot, \cdot)$  with  $\gamma$ .

It is known [17] that the eigenvalues defined by (4.2) has the structure of  $E_M \cup \gamma E_L$ , where  $E_M$  is the set of Maxwell eigenvalues and  $E_L$  is the set of Laplace eigenvalues with homogeneous Dirichlet boundary condition. Therefore, for  $\gamma = h^{-2}$  (Eigensolver 2) or  $\gamma = h^{-1}$  (variant eigensolver), the lower ranges of the spectra defined by (1.1) and (4.2) become identical as  $h \downarrow 0$  (i.e.,  $\gamma \uparrow \infty$ ), and the Maxwell eigenvalues can be captured by either scheme with second order accuracy.

### 4.2.3 Results for the doubly connected domain

As mentioned at the end of Section 2, Eigensolver 2 can be applied to multiply connected domains. Here we consider the doubly connected domain  $(0, 4)^2 \setminus (1, 3)^2$ , where the meshes are graded around the re-entrant corners with grading parameter  $\frac{1}{3}$  (Figure 4.3, right).

Table 4.5: First 5 numerical eigenvalues on the doubly connected domain  $(0, 4)^2 \setminus (1, 3)^2$  computed by Eigensolver 2 using graded meshes

$n = \frac{1}{h}$	the 1 <sup>st</sup>	the 2 <sup>nd</sup>	the 3 <sup>rd</sup>	the 4 <sup>th</sup>	the 5 <sup>th</sup>
2	0.716	0.925	0.925	1.301	2.896
4	0.396	0.661	0.661	1.146	2.200
8	0.175	0.471	0.471	1.080	1.784
16	0.063	0.373	0.373	1.054	1.586
32	0.020	0.335	0.335	1.045	1.511
64	0.006	0.322	0.322	1.042	1.486

Numerical results for the first 5 Maxwell eigenvalues computed by Eigensolver 2 are reported in Table 4.5, from which we can see that the scheme captures the zero Maxwell eigenvalue whose multiplicity is 1.

Note that Maxwell eigensolvers based on the formulation (1.2) must face the problem of separating the true Maxwell eigenvalue 0 from the spurious zero eigenvalues.

### 4.3 Numerical results for Eigensolver 3

In this subsection we present numerical results for Eigensolver 3. We will focus on the accuracy of the scheme, the role played by the two last terms in the definition of  $c_{h,0}(\cdot, \cdot)$ , and the performance of the scheme on non-conforming meshes. Results similar to those reported in Section 4.1.2 for Eigensolver 1 and those in Section 4.2.3 for Eigensolver 2 also hold for Eigensolver 3 and will not be repeated here.

#### 4.3.1 Accuracy of the scheme

In the first experiment we compute the Maxwell eigenvalues for the square  $(0, \pi)^2$  using conforming uniform meshes. Figure 4.10 contains the plot of the first 20 numerical eigenvalues versus the parameter  $n = \pi/h$ , which shows that the eigenvalues are well resolved and there is no spurious eigenmode. The performance of this solver is not quite as good as Eigensolver 1 and Eigensolver 2 for meshes that are relatively coarse.

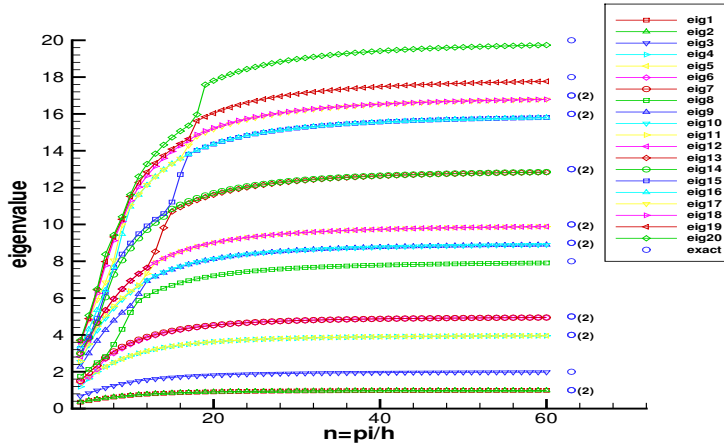


Figure 4.10: First 20 Maxwell eigenvalues for  $(0, \pi)^2$  computed by Eigensolver 3 using conforming uniform meshes

We can also see from Table 4.6 that the numerical approximations converge with second order accuracy, which confirms our error estimate (3.8). In the second experiment we compute the Maxwell eigenvalues for the  $L$ -shaped domain using graded meshes. Table 4.7 contains the first 5 numerical eigenvalues which shows that the scheme has second order accuracy.

Results for the first 10 Maxwell eigenvalues are plotted in Figure 4.11, from which one can see that there is no spurious eigenmode.

Table 4.6: First 5 Maxwell eigenvalues for  $(0, \pi)^2$  computed by Eigensolver 3 using conforming uniform meshes

$n = \frac{\pi}{h}$	the 1 <sup>st</sup>	order	the 2 <sup>nd</sup>	order	the 3 <sup>rd</sup>	order	the 4 <sup>th</sup>	order	the 5 <sup>th</sup>	order
4	0.347	-	0.367	-	0.673	-	1.188	-	1.409	-
8	0.626	0.80	0.634	0.79	1.239	0.80	2.495	0.90	2.496	0.78
16	0.863	1.45	0.866	1.45	1.723	1.46	3.446	1.44	3.446	1.44
32	0.962	1.84	0.963	1.84	1.923	1.84	3.845	1.83	3.845	1.83
64	0.990	1.97	0.990	1.97	1.980	1.97	3.960	1.96	3.960	1.96
128	0.998	1.97	0.998	2.00	1.995	2.01	3.990	1.99	3.990	1.99
Exact	1		1		2		4		4	

Table 4.7: First 5 Maxwell eigenvalues for the L-shaped domain  $(-0.5, 0.5)^2 \setminus [0, 0.5]^2$  computed by Eigensolver 3 using graded meshes

$n = \frac{1}{2h}$	the 1 <sup>st</sup>	order	the 2 <sup>nd</sup>	order	the 3 <sup>rd</sup>	order	the 4 <sup>th</sup>	order	the 5 <sup>th</sup>	order
2	2.626	-	3.442	-	5.087	-	5.174	-	5.656	-
4	4.747	1.50	9.963	1.36	11.233	0.28	11.316	0.28	12.226	0.26
8	5.574	1.81	13.102	2.01	30.631	1.67	36.653	3.32	38.548	2.25
16	5.819	1.98	13.875	1.98	37.008	1.84	38.822	2.11	44.091	2.26
32	5.882	2.02	14.071	2.00	38.847	1.97	39.319	2.04	45.204	2.05
Exact	5.902		14.136		39.478		39.478		45.558	

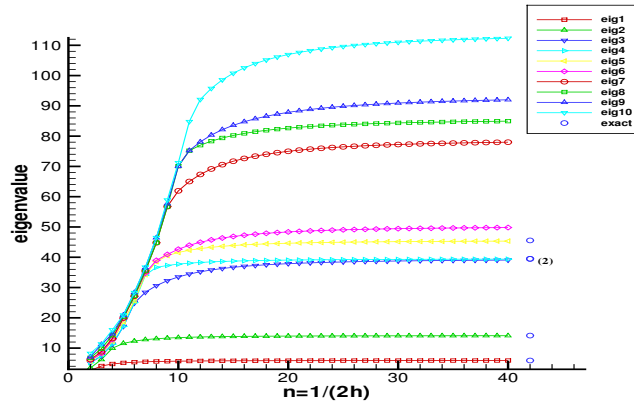


Figure 4.11: First 10 Maxwell eigenvalues for the L-shaped domain computed by Eigensolver 3 using graded meshes

**4.3.2 The role of the last two terms in (2.9)**

The last two penalization terms in the bilinear form  $c_{h,0}(\cdot, \cdot)$  are included to compensate for the lack of any continuity for the vector fields in the space  $U_h$ . Numerical examples in [10] indicate that without these two terms the numerical scheme for the source problem (1.3) will fail to converge. In this subsection we examine the numerical spectrum of the variant of Eigensolver 3 where the last two penalization terms in (2.9) are absent.

The first 40 eigenvalues for the square  $(0, \pi)^2$  computed by the variant eigensolver using conforming uniform meshes are presented in Figure 4.12. One can see that there are many spurious eigenvalues, which again confirms the necessity of these two penalization terms.

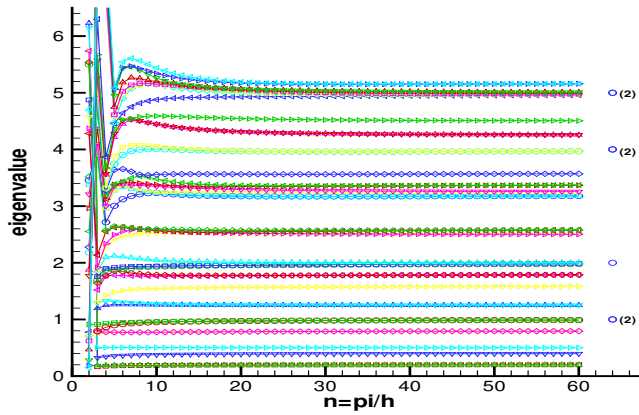


Figure 4.12: First 40 numerical eigenvalues for  $(0, \pi)^2$  computed by the variant of Eigensolver 3 where the last two terms in (2.9) are absent

**4.3.3 Results with nonconforming meshes**

As mentioned at the end of Section 2, Eigensolver 3 can be implemented on both conforming and nonconforming meshes. In this subsection we present numerical results for the square  $(0, \pi)^2$  using the nonconforming mesh depicted in Figure 4.1 (right), where the square domain  $\Omega = (0, \pi)^2$  is first divided into  $\Omega_1 = (0, \frac{\pi}{2}) \times (0, \pi)$  and  $\Omega_2 = (\frac{\pi}{2}, \pi) \times (0, \pi)$  and then conforming meshes are introduced on  $\Omega_1$  and  $\Omega_2$  separately so that the overall mesh on  $\Omega$  is nonconforming. For such meshes, we define  $\mathcal{E}_h$  by

$$\mathcal{E}_h = \{e \in \partial T : T \in \mathcal{T}_h \text{ and } T \subset \Omega_1\} \cup \{e \in \partial T \setminus \Gamma : T \in \mathcal{T}_h \text{ and } T \subset \Omega_2\},$$

where  $\Gamma = \partial\Omega_1 \cap \partial\Omega_2$ . The subset of  $\mathcal{E}_h$  interior to  $\Omega$  is denoted by  $\mathcal{E}_h^i$ .

Table 4.8 contains the first 5 Maxwell eigenvalues computed by Eigensolver 3 using these nonconforming meshes. It shows that Eigensolver 3 remains second order accurate and its performance is comparable with the performance on conforming meshes (Table 4.6).

Table 4.8: First 5 Maxwell eigenvalues for  $(0, \pi)^2$  computed by Eigensolver 3 using nonconforming meshes

$n = \frac{\pi}{h}$	the 1 <sup>st</sup>	order	the 2 <sup>nd</sup>	order	the 3 <sup>rd</sup>	order	the 4 <sup>th</sup>	order	the 5 <sup>th</sup>	order
4	0.331	-	0.349	-	0.652	-	1.077	-	1.307	-
8	0.603	0.75	0.611	0.74	1.200	0.75	2.389	0.86	2.433	0.78
16	0.851	1.41	0.853	1.40	1.699	1.41	3.392	1.41	3.404	1.39
32	0.958	1.82	0.958	1.81	1.915	1.82	3.828	1.82	3.830	1.81
64	0.990	1.96	0.989	1.96	1.978	1.96	3.956	1.96	3.956	1.96
128	0.997	1.99	0.997	1.99	1.995	1.99	3.989	1.99	3.989	1.99
Exact	1		1		2		4		4	

## 5 Detection of Spurious Eigenmodes

In this section we discuss numerical techniques that can detect the spurious eigenmodes generated by the T-type and N-type variants of Eigensolver 1 introduced in Section 4.1.2 and turn these variants into effective Maxwell eigensolvers. These techniques may also contribute to the development of methods that can detect spurious eigenmodes generated by other Maxwell eigensolvers (cf. for example [6, 22]).

Given  $\mathbf{w} \in V_h$ , we define

$$|\mathbf{w}|_{t,h} = \left\{ \sum_{e \in \mathcal{E}_h} \frac{[\Phi_\mu(e)]^2}{|e|} \int_e \llbracket \mathbf{w} \rrbracket_t^2 ds \right\}^{1/2}, \quad (5.1)$$

$$|\mathbf{w}|_{\text{div},h} = \left\{ \sum_{e \in \mathcal{E}_h^i} \frac{[\Phi_\mu(e)]^2}{|e|} \int_e \llbracket \mathbf{w} \rrbracket_n^2 ds \right\}^{1/2}. \quad (5.2)$$

Note that  $|\mathbf{w}|_{t,h}$  measures the conformity of  $\mathbf{w}$  with respect to the space  $H_0(\text{curl}; \Omega)$ , while  $|\mathbf{w}|_{\text{div},h}$  measures the conformity of  $\mathbf{w}$  with respect to the space  $H(\text{div}; \Omega)$  (and hence the space  $H(\text{div}^0; \Omega)$ , since vector fields in  $V_h$  are locally divergence-free).

Since the Maxwell eigenfunctions defined by (1.1) belong to  $H_0(\text{curl}; \Omega) \cap H(\text{div}^0; \Omega)$ , in order for a sequence of discrete eigenfunctions  $\{\mathbf{v}_h\}_h \subset V_h$

to approximate an eigenfunction, the following conditions are necessary:

$$\lim_{h \rightarrow 0} |\mathbf{v}_h|_{t,h} = 0, \tag{5.3}$$

$$\lim_{h \rightarrow 0} |\mathbf{v}_h|_{\text{div},h} = 0. \tag{5.4}$$

This is confirmed by examining the log-log plot of  $|\hat{\mathbf{u}}_h|_{\text{div},h}$  (resp.  $|\hat{\mathbf{u}}_h|_{t,h}$ ) versus  $n = \pi/h$  on the left (resp. right) side of the top row of Figure 5.1, where  $\hat{\mathbf{u}}_h$  is the discrete eigenfunction for the square  $(0, \pi)^2$  computed by Eigensolver 1 and normalized so that  $\|\hat{\mathbf{u}}_h\|_{L_2(\Omega)} = 1$ . We can see that both  $|\hat{\mathbf{u}}_h|_{\text{div},h}$  and  $|\hat{\mathbf{u}}_h|_{t,h}$  for the discrete eigenfunctions corresponding to the first 20 discrete eigenvalues decay steadily to 0, mirroring the fact that the discrete eigenfunctions computed by Eigensolver 1 converge to the Maxwell eigenfunctions (Theorem 3.1).

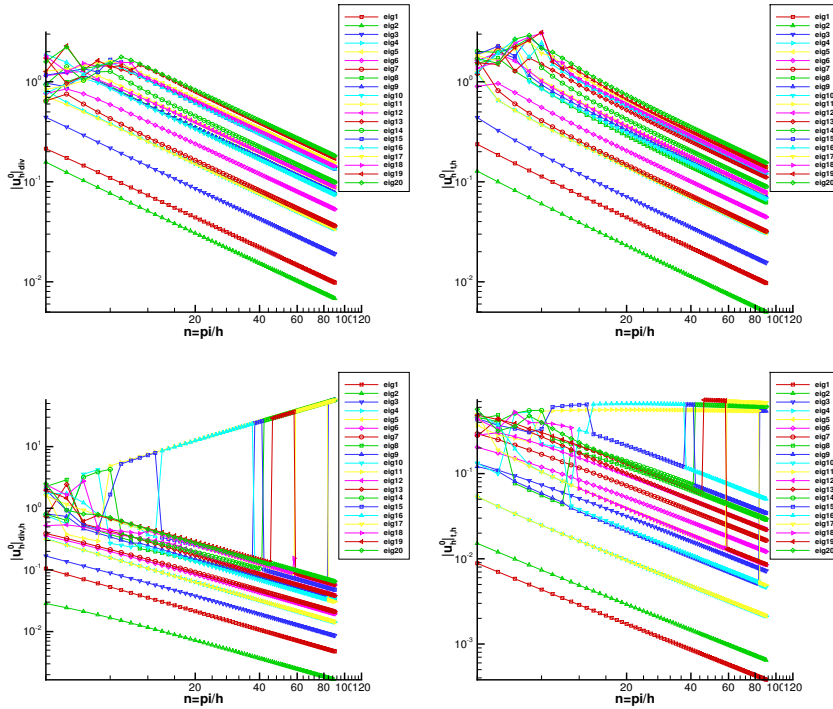


Figure 5.1: Log-log plots of  $|\hat{\mathbf{u}}_h|_{\text{div},h}$  (left) and  $|\hat{\mathbf{u}}_h|_{t,h}$  (right) versus  $n$ , where  $n = \pi/h$ , for the TN-type eigensolver (top, with  $C_{p,n} = C_{p,t} = 1$  in (4.1)) and the T-type eigensolver (bottom, with  $C_{p,n} = 0$  and  $C_{p,t} = 30$  in (4.1)) on the square  $(0, \pi)^2$  with conforming uniform meshes

We have also computed the first 20 eigenvalues for the square  $(0, \pi)^2$  by the T-type variant of Eigensolver 1 defined by (4.1) with  $C_{p,n} = 0$  and  $C_{p,t} = 30$ . On the bottom row of Figure 5.1, we present the log-log plots of  $|\hat{\mathbf{u}}_h|_{\text{div},h}$  (left) and  $|\hat{\mathbf{u}}_h|_{t,n}$  (right) versus  $n = \pi/h$ , where the  $\hat{\mathbf{u}}_h$ 's are the normalized discrete eigenfunction. We can see that (5.3) and (5.4) hold for some but not all discrete eigenfunctions, which agree with the plot on the left-hand side of the middle row of Figure 4.6 that demonstrate the existence of spurious eigenmodes for the T-type variant.

To better understand the behavior of these numerical eigenfunctions, we present the data in a different way in Figure 5.2, where bright colors indicate the violation of (5.4) (left) or (5.3) (right). Based on Figure 5.1 and Figure 5.2, we can assert, for example, that (i) when  $n = 50$ , the 11th, 14th, 19th numerical eigenvalues are spurious, (ii) when  $n = 70$ , the 11th, 14th and 17th numerical eigenvalues are spurious, and (iii) when  $n = 85$ , the 9th, 14th and 15th numerical eigenvalues are spurious. These assertions agree with the results in Figure 4.6. Under a more careful examination of the numerical results, one can conclude that (5.3) and (5.4) are necessary and sufficient for the numerical eigenvalues computed by the T-type variant of Eigensolver 1 to be physical (i.e., non-spurious) Maxwell eigenvalues.

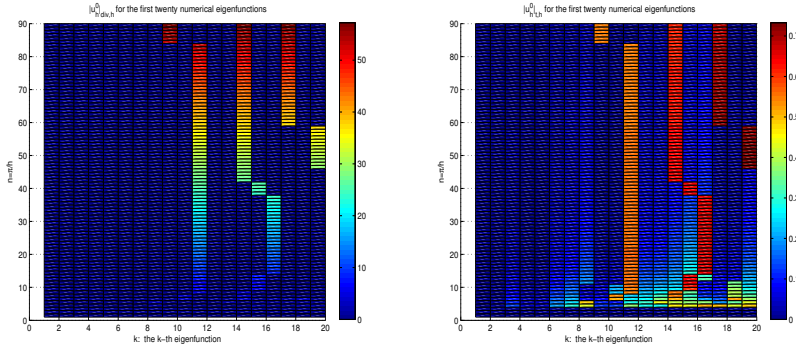


Figure 5.2:  $|\hat{\mathbf{u}}_h|_{\text{div},h}$  (left) and  $|\hat{\mathbf{u}}_h|_{t,h}$  (right) versus different  $n = \pi/h$ , for normalized discrete eigenfunctions corresponding to the first 20 numerical eigenvalues computed by the T-type variant of Eigensolver 1 (with  $C_{p,n} = 0$  and  $C_{p,t} = 30$  in (4.1)) for the square  $(0, \pi)^2$  using conforming uniform meshes

We have also performed a similar numerical study for the L-shape domain, computing the first 10 discrete eigenvalues by the TN-type, T-type and N-type variants using graded meshes. The plots in Figure 5.3 and Figure 5.4 confirm that both the TN-type and T-type variants produce ac-

curate approximations for the Maxwell eigenvalues. The same holds for the N-type variant, except for the 3 spurious zero eigenvalues. These results are consistent with the plots in Figure 4.7.

Similar tests can also be performed for the variants of Eigensolver 2 and Eigensolver 3, as long as the definitions of (5.1) and (5.2) are modified accordingly. For instance, to detect spurious eigenmodes for the variants of Eigensolver 2, one needs to modify the definition of (5.2) to include the numerical divergence contributed by  $\sum_{T \in \mathcal{T}_h} \|\nabla_h \cdot \mathbf{w}\|_{L_2(T)}^2$ .

## 6 Concluding Remarks

Our previous work [9, 10, 11] on the source problem for the time-harmonic Maxwell equations indicates that the Maxwell eigenproblem (1.1) can also be solved by nonconforming finite element methods. However, only Eigensolver 3 has been analyzed in [10]. In this paper we have presented a unified analysis and performed thorough numerical tests for all three nonconforming Maxwell eigensolvers.

Our results show that these Maxwell eigensolvers have optimal order convergence on properly graded meshes and they do not generate any spurious eigenmodes even on relatively coarse meshes. Furthermore, they impose just the right amount of continuity across element interfaces without having to choose any parameters.

We have demonstrated the capability of these eigensolvers for multiply connected domains and nonconforming meshes. We have also developed numerical techniques that can detect the spurious eigenmodes generated by some variants of these eigensolvers.

The extension of these schemes to three dimensional electromagnetic problems and the development of fast solvers for these schemes are subjects of our on going research.

**Acknowledgment** The authors would like to thank Guido Kanschat for helpful discussions concerning the material in Section 5.

## References

- [1] F. Assous, P. Ciarlet, Jr. and E. Sonnendrücker, *Resolution of the Maxwell equation in a domain with reentrant corners*. M<sup>2</sup>AN, 32:359–389, 1998.
- [2] I. Babuška and J. Osborn, *Eigenvalue Problems*, In P.G. Ciarlet and J.L. Lions, editors, handbook of Numerical Analysis II 641–787. North-Holland, Amsterdam, 1991.

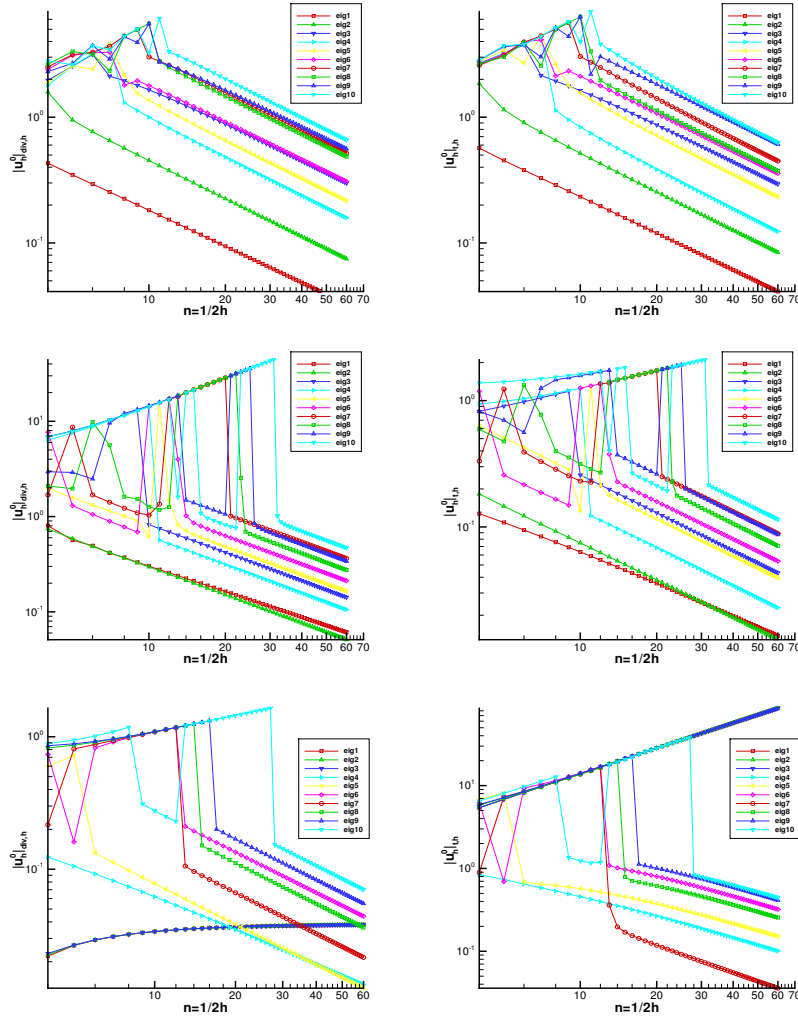


Figure 5.3: Log-log plots of  $|\hat{\mathbf{u}}_h|_{\text{div},h}$  (left) and  $|\hat{\mathbf{u}}_h|_{t,n}$  (right) versus  $n$ , where  $n = 1/(2h)$ , for the TN-type eigensolver (top, with  $C_{p,n} = C_{p,t} = 1$  in (4.1)) the T-type eigensolver (middle, with  $C_{p,n} = 0$  and  $C_{p,t} = 25$  in (4.1)) and the N-type eigensolver (bottom, with  $C_{p,n} = 25$  and  $C_{p,t} = 0$  in (4.1)) on the L-shape domain with graded meshes

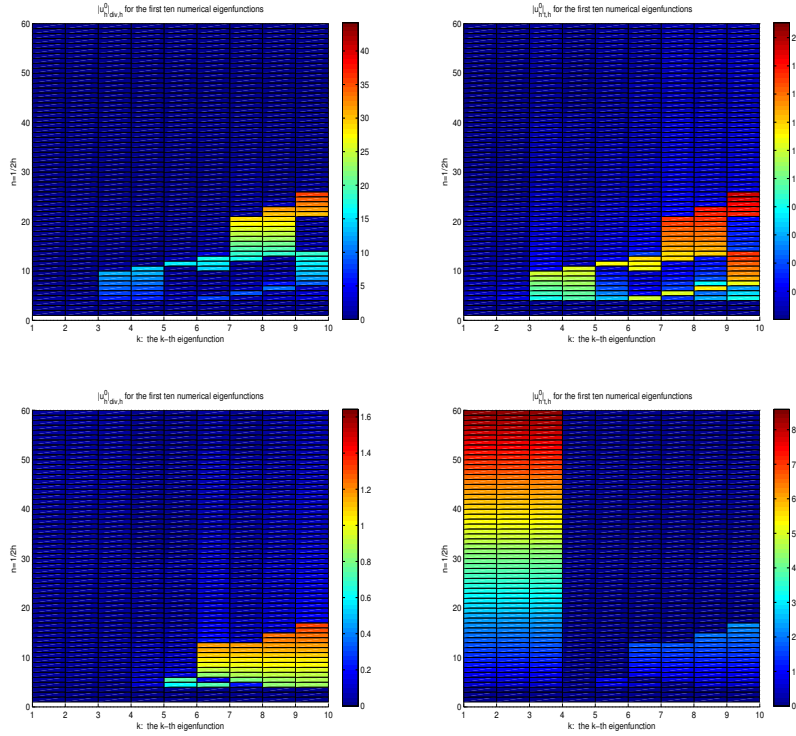


Figure 5.4:  $|\hat{\mathbf{u}}_h|_{\text{div},h}$  (left) and  $|\hat{\mathbf{u}}_h|_{t,h}$  (right) versus different  $n = 1/(2h)$ , for normalized discrete eigenfunctions corresponding to the first 10 numerical eigenvalues computed by the T-type variant of Eigensolver 1 (top, with  $C_{p,n} = 0$  and  $C_{p,t} = 25$  in (4.1)) and the N-type variant of Eigensolver 1 (bottom, with  $C_{p,n} = 25$  and  $C_{p,t} = 0$  in (4.1)) for the L-shaped domain using graded meshes

- [3] D. Boffi. Fortin operators and discrete compactness for edge elements, *Numer. Math.*, 87 (2000), 229–246.
- [4] D. Boffi. Approximation of eigenvalues in mixed form, discrete compactness property, and application to  $hp$  mixed finite elements, *Comput. Methods Appl. Mech. Engrg.*, 196 (2007), 3672–3681.
- [5] D. Boffi, F. Brezzi, and L. Gastaldi. On the convergence of eigenvalues for mixed formulations, *Ann. Scuola Norm. Sup. Pisa Cl. Sci. (4)*, 25 (1997), 131–154.

- [6] D. Boffi, P. Fernandes, L. Gastaldi and I. Perugia, *Computational models of electromagnetic resonators: analysis of edge element approximation*, SIAM J. Numer. Anal. 36 (1999), 1264–1290.
- [7] D. Boffi, F. Kikuchi, and J. Schöberl. Edge element computation of Maxwell’s eigenvalues on general quadrilateral meshes, *Math. Models Methods Appl. Sci.*, 16 (2006), 265–273.
- [8] S.C. Brenner, J.Cui, F. Li and L.-Y. Sung, *A nonconforming finite element method for a two-dimensional curl-curl and grad-div problem*, *Numer. Math.*, (2008), DOI:10.1007/s00211-008-0149-7.
- [9] S. C. Brenner, F. Li and L.-Y. Sung, *A locally divergence-free nonconforming finite element method for the reduced time-harmonic Maxwell equations*, *Math. Comp.* 76 (2007), 573-595.
- [10] S. C. Brenner, F. Li and L.-Y. Sung, *A locally divergence-free interior penalty method for two-dimensional curl-curl problems*, SIAM J. Numer. Anal. 46 (2008), 1190–1211,
- [11] S. C. Brenner, F. Li and L.-Y. Sung, *A nonconforming penalty method for two dimensional curl-curl problems*, preprint.
- [12] A. Buffa and I. Perugia, *Discontinuous Galerkin approximation of the Maxwell eigenproblem*, SIAM J. Numer. Anal., 44 (2006), 2198-2226.
- [13] S. Caorsi, P. Fernandes and M. Raffetto, *On the convergence of Galerkin finite element approximations of electromagnetic eigenproblems*, SIAM J. Numer. Anal., 38 (2000), 580–607.
- [14] S. Caorsi, P. Fernandes and M. Raffetto, *Spurious-free approximations of electromagnetic eigenproblems by means of Nédélec-type elements*, M2AN, 35 (2001), 331–358.
- [15] F. Chatelin, *Spectral Approximations of Linear Operators*, Academic Press, New York, 1983.
- [16] M. Costabel, *A Remark on the Regularity of Solutions of Maxwell’s Equations on Lipschitz Domains*, *Math. Methods Appl. Sci.* 12 (1990), 365–368.
- [17] M. Costabel and M. Dauge, *Maxwell and Lamé eigenvalues on polyhedra*, *Math. Methods Appl. Sci.*, 22 (1999), 243–258.
- [18] M. Costabel and M. Dauge, *Singularities of electromagnetic fields in polyhedral domains*. *Arch. Ration. Mech. Anal.*, 151 (2000), 221–276.

- [19] M. Costabel and M. Dauge, *Weighted regularization of Maxwell equations in polyhedral domains*. Numer. Math., 93 (2002), 239–277.
- [20] M. Crouzeix and P.-A. Raviart, *Conforming and nonconforming finite element methods for solving the stationary Stokes equations I*. RAIRO Anal. Numér., 7 (1973), 33–75.
- [21] N. Dunford and J.T. Schwartz, *Linear Operators II*, Wiley-Interscience, New York, 1963.
- [22] J.S. Hesthaven and T. Warburton, *High order nodal discontinuous Galerkin methods for the Maxwell eigenvalue problem*, Philos. Trans. Roy. Soc. London Ser. A. 362 (2004). 493-524.
- [23] T. Kato. *Perturbation Theory of Linear Operators*, Springer-Verlag, Berlin, 1966.
- [24] P. Monk, *Finite element methods for Maxwell's equations. Numerical Mathematics and Scientific Computation*, Oxford University Press, New York, 2003.
- [25] T. Warburton and M. Embree, *On the role of the penalty in the local discontinuous Galerkin method for Maxwell's eigenvalue problem*, Comp. Mech. Appl. Eng., 195 (2006), 3205-3223.